

NEW ADVANCES IN THE STUDY OF GENERALIZED WILLMORE SURFACES AND FLOW

BHAGYA ATHUKORALLAGE, EUGENIO AULISA, GIORGIO BORNIA,
THANUJA PARAGODA and MAGDALENA TODA

*Department of Mathematics and Statistics, Texas Tech University
79409-1042 Lubbock, TX, USA*

Abstract. In this paper we study a Generalized Willmore flow for graphs and its numerical applications. First, we derive the time dependent equation which describes the geometric evolution of a Generalized Willmore flow in the graph case. This equation is recast in divergence form as a coupled system of second order nonlinear PDEs. Furthermore, we study finite element numerical solutions for steady-state cases obtained with the help of the FEMuS library (Finite Element Multiphysics Solver). We use automatic differentiation (AD) tools to compute the exact Jacobian of the coupled PDE system subject to Dirichlet boundary conditions.

MSC: 35R01, 49Q20, 53A10, 53Z05, 58J32, 65N30

Keywords: Numerical solutions of Willmore type equations, Willmore flow, Willmore surfaces

1. Introduction

Let M be a smooth immersed surface in \mathbb{R}^3 . We consider the Generalized Willmore energy functional

$$W = \int_M (aH^2 + b) dS$$

where $a = 2k_c$ represents the double of the usual bending rigidity and b is the surface tension coefficient. The term dS is the area element with respect to the induced metric. Then, the corresponding Euler-Lagrange equation is given by

$$\Delta H + 2(H^2 - K - \epsilon)H = 0$$

where $\epsilon = b/a$ and Δ is the Laplace-Beltrami operator corresponding to the natural metric [1]. The Willmore functional and its generalizations play a prominent role in differential geometry [8, 11, 12]. These generalizations include the Helfrich energy for lipid bilayers, in which bending rigidities are established as multiplicative constants of the mean curvature H and the Gauss curvature K , while neglecting the surface tension of the membranes. In this study, our Generalized Willmore energy is a composition of the classical bending energy (Willmore energy) and the energy due to the surface tension. Recently, Willmore-type energies and Willmore-type surfaces in space forms were studied in [2] in which the authors proved that Willmore-type immersions in different space forms essentially satisfy the same PDE (Willmore-type equation).

In this paper we address the Generalized Willmore flow for graphs which was recently studied by other authors over the past decades [5]. The paper is organized as follows. In Section 2 we first obtain a formulation to a Generalized Willmore flow equation for evolving surfaces. This fourth order Generalized Willmore flow equation, together with the mean curvature formula for a graph, form a coupled PDE system. Our final goal is to numerically solve this PDE system corresponding to the Generalized Willmore flow based on finite element methods. Our coupled PDE system can be linearized in practice with automatic differentiation tools. In Section 3, we provide non trivial solutions which are induced by a Clifford torus for the coupled PDE system subject to the Dirichlet boundary conditions and then the convergence results and graphical figures are presented for the Generalized Willmore flow for graphs at the steady case.

2. Generalized Willmore Flow

Let us briefly review the literature on Willmore flow which is the L^2 -gradient flow corresponding to the Willmore energy. The Willmore flow usually occurs in digital geometry processing, geometric modeling, and physical simulation. Recently, the authors [4] studied the discrete Willmore energy and its flow and they derived the relevant gradient expressions including a linearization (approximation of the Hessian), which are required for nonlinear numerical solvers. In [3], Barrett, Garcke, and Nurnberg presented a parametric approximation of Willmore flow and related geometric evolution equations and they provided numerous numerical experiments, including simulations for energies appearing in the modelling of biological cell membranes. In 2004, a level set formulation for Willmore flow was derived by Droske and Rumpf and they used gradient flow perspective and generalized the metric to sets of level set surfaces using the identification of normal velocities and variations of the level set function in time via the level set equation [7]. Several papers [6, 10] the authors analyzed the error estimates for the Willmore flow of graphs along with numerical experiments. For instance, Ji and

Xu [10] analyzed a local discontinuous Galerkin method for the Willmore flow of graphs on Cartesian meshes. In [5], Deckelnick, Dziuk and Elliott provided a computation of geometric partial differential equations and mean curvature flow in a precise way. In 2015, a C^1 -finite element method for the Willmore flow of two-dimensional graphs subject to Dirichlet boundary conditions was introduced by Deckelnick, Katz, and Schieweck. They proved quasi-optimal error bounds in Sobolev norms for the solution and its time derivative [6]. These papers motivated us to provide a numerical approach for our Generalized Willmore flow for graphs. We are interested in reformulating a Generalized Willmore flow equation of graphs and presenting a numerical approach using automatic differentiation.

Let us consider the evolution of a two-dimensional surface $M(t)$ which is embedded in \mathbb{R}^3 and described as a graph of function $u : (0, T) \times \Omega \rightarrow \mathbb{R}$, $\Omega \subset \mathbb{R}^2$ where Ω is an open domain. Then we consider the following geometric evolution equation which is the Generalized Willmore flow equation

$$V = \Delta H + 2(H^2 - K - \epsilon)H \tag{1}$$

on $M(t)$, where V is the normal velocity of the evolving surfaces $M(t)$ corresponding to the Generalized Willmore energy

$$W(M) = \int_M (H^2 + \epsilon) \, dS$$

for an immersed surface M in \mathbb{R}^3 [2]. The surface M is evolving in time to follow variations of steepest descent of the energy. It is a fourth-order flow, since the variation of the energy contains fourth-order derivatives.

2.1. The Graph Case

For every $t \in [0, T]$ let $M(t) = \{(x, y, U(x, y, t)) ; (x, y) \in \Omega \subset \mathbb{R}^2\}$ be the graph of U . Recall that the Laplace-Beltrami operator is given by the formula

$$\Delta = \frac{1}{A} \nabla \cdot \left(\left(AI - \frac{\nabla U (\nabla U)^T}{A} \right) \nabla \right)$$

where $A = \sqrt{1 + |\nabla U|^2} = \sqrt{1 + U_x^2 + U_y^2}$.

ΔH can be expressed as in the matrix form

$$\Delta H = \frac{1}{A} \nabla \cdot \left(\frac{1}{A} \begin{pmatrix} 1 + U_y^2 & -U_x U_y \\ -U_x U_y & 1 + U_x^2 \end{pmatrix} \nabla H \right). \tag{2}$$

We can rewrite (2) as

$$\Delta H = \nabla \cdot \left(\frac{1}{A} \left(I - \frac{\nabla U (\nabla U)^T}{A^2} \right) \nabla (AH) \right) - H \nabla \cdot \left(\frac{1}{A} \left(I - \frac{\nabla U (\nabla U)^T}{A^2} \right) \nabla A \right).$$

Using

$$2H = \nabla \cdot \left(\frac{\nabla U}{A} \right) \quad (3)$$

we obtain

$$\frac{1}{A} \left(I - \frac{\nabla U (\nabla U)^T}{A^2} \right) \nabla A = \frac{1}{A} \left(\nabla A - \frac{\Delta U}{A} \nabla U \right) + 2H \frac{\nabla U}{A}. \quad (4)$$

It is straightforward to verify that

$$\nabla \cdot \left(\frac{1}{A} \left(\nabla A - \frac{\Delta U}{A} \nabla U \right) \right) = -2K. \quad (5)$$

Using (4) and (5) we can express (2) as

$$\Delta H = \nabla \cdot \left(\frac{1}{A} \left(I - \frac{\nabla U (\nabla U)^T}{A^2} \right) (\nabla AH) \right) + 2HK - 2H \nabla \cdot \left(H \frac{\nabla U}{A} \right) \quad (6)$$

$$\Delta H = \nabla \cdot \left(\frac{1}{A} \left(I - \frac{\nabla U (\nabla U)^T}{A^2} \right) (\nabla AH) \right) + 2HK - \nabla \cdot \left(H^2 \frac{\nabla U}{A} \right) - 2H^3.$$

By substituting (6) in (1) we obtain the fourth order PDE given by

$$V - \nabla \cdot \left(\frac{1}{A} \left(I - \frac{\nabla U (\nabla U)^T}{A^2} \right) (\nabla AH) \right) + \nabla \cdot \left(H^2 \frac{\nabla U}{A} \right) + 2H\epsilon = 0. \quad (7)$$

Using (3) we rewrite (7) as

$$U_t - A \nabla \cdot \left(\frac{1}{A} \left(I - \frac{\nabla U (\nabla U)^T}{A^2} \right) (\nabla AH) - H^2 \frac{\nabla U}{A} - \epsilon \left(\frac{\nabla U}{A} \right) \right) = 0 \quad (8)$$

where $V = U_t/A$. We express (1) in divergence form using the Gauss curvature formula of a graph as shown in (8). The important point is that the Gauss curvature does not appear in the fourth-order PDE. Then we transform the above fourth order PDE into a coupled system of two nonlinear second order PDEs as in [5, 7].

Define

$$W := \frac{A}{2} \nabla \cdot \left(\frac{\nabla U}{A} \right) = AH$$

$$B := I - \frac{\nabla U (\nabla U)^T}{A^2} = \frac{1}{1 + U_x^2 + U_y^2} \begin{pmatrix} 1 + U_y^2 & -U_x U_y \\ -U_x U_y & 1 + U_x^2 \end{pmatrix}.$$

We refer to W as *weighted mean curvature*. Then (8) becomes as a coupled system of two nonlinear second order PDEs with respect to two unknowns U and W

$$\begin{aligned}
 U_t &= A \nabla \cdot \left(\frac{B}{A} \nabla W - \frac{W^2}{A^3} \nabla U - \epsilon \left(\frac{\nabla U}{A} \right) \right) \\
 W &= \frac{A}{2} \nabla \cdot \left(\frac{\nabla U}{A} \right).
 \end{aligned}$$

2.2. Steady-State Weak Formulation

In this part of the paper we describe how we obtain the steady state weak formulation for the above coupled PDE system. From now on we set $U_t = 0$ in (9). Now we multiply (9) and (9) by test functions $\varphi, \psi \in H_0^1(\Omega)$ respectively and apply integration by parts we obtain the following system

$$\begin{aligned}
 & - \int_{\Omega} \frac{B}{A} \nabla W \cdot \nabla \varphi \, d\Omega + \int_{\Gamma} \frac{B}{A} \nabla W \cdot \nu \varphi \, d\Gamma + \int_{\Omega} \frac{W^2}{A^3} \nabla U \cdot \nabla \varphi \, d\Omega \\
 & - \int_{\Gamma} \frac{W^2}{A^3} \nabla U \cdot \nu \varphi \, d\Gamma + \int_{\Omega} \epsilon \frac{\nabla U}{A} \cdot \nabla \varphi \, d\Omega - \int_{\Gamma} \epsilon \frac{\nabla U}{A} \cdot \nu \varphi \, d\Gamma = 0 \\
 & - \int_{\Omega} \frac{\nabla U}{A} \nabla \psi \, d\Omega + \int_{\Gamma} \frac{\nabla U}{A} \cdot \nu \psi \, d\Gamma = \int_{\Omega} 2 \frac{W}{A} \psi \, d\Omega
 \end{aligned}$$

where Γ is the boundary of Ω . In the case of Dirichlet boundary conditions the boundary terms vanish in the above formulation because of the choice of the test functions φ and ψ .

Hence, the weak formulation of the steady-state Generalized Willmore flow graph is given by

$$\begin{aligned}
 \int_{\Omega} \left(- \frac{B}{A} \nabla W \cdot \nabla \varphi + \left(\frac{W^2}{A^3} + \frac{\epsilon}{A} \right) \nabla U \cdot \nabla \varphi \right) d\Omega &= 0, \quad \varphi \in H_0^1(\Omega) \\
 \int_{\Omega} \left(\frac{2W}{A} \psi + \frac{\nabla U}{A} \cdot \nabla \psi \right) d\Omega &= 0, \quad \psi \in H_0^1(\Omega)
 \end{aligned} \tag{9}$$

with prescribed Dirichlet boundary conditions $U(\Gamma) = U_0$ and $W(\Gamma) = W_0$.

3. Numerical Results

The above nonlinear coupled PDE system is solved by using a Newton scheme. The implementation of the Jacobian matrix in the nonlinear iterations is challenging because of the complexity of the operators. Therefore we make use of Automatic Differentiation (AD) tools (sometimes called algorithmic differentiation or computational differentiation), which are a set of techniques to evaluate the derivative of a function specified by a computer program.

3.1. Automatic Differentiation (AD) for the Generalized Willmore Flow

Let $\mathbf{v} = (U, W)$ and we rewrite (9) in compact notation as

$$\mathbf{F}(\mathbf{v}) = 0.$$

Let \mathbf{v}_0 be an initial guess. Then a single Newton iteration is given by

$$\mathbf{v}_n = \mathbf{v}_{n-1} - \mathbf{J}^{-1}(\mathbf{v}_{n-1})\mathbf{F}(\mathbf{v}_{n-1}) \quad \text{for } n \geq 1$$

and it is repeated until $\|\mathbf{v}_n - \mathbf{v}_{n-1}\| < \epsilon$. Here, $\mathbf{J}(\mathbf{v}_n) = \frac{\partial \mathbf{F}}{\partial \mathbf{v}}(\mathbf{v}_n)$. Automatic differentiation exploits the fact that every computer program, no matter how complicated, executes a sequence of elementary arithmetic operations (addition, subtraction, multiplication, division, etc.) and elementary functions (exp, log, sin, cos, etc.). By applying the chain rule repeatedly to these operations, derivatives of arbitrary order can be computed automatically accurately to working precision. In our work we have chosen to use the Adept software library, which enables algorithms written in C++ to be automatically differentiated using an operator overloading strategy. The full Jacobian matrix can be computed with very little code modification [9].

3.2. The Clifford Torus as a Steady-State Solution of the Willmore Flow

In order to validate our numerical algorithm, we have compared steady-state Willmore flow solutions with known analytical solutions. We have tested not only that each solution converges to the corresponding analytic one, but also that the theoretical convergence order is recollect for $h \rightarrow 0$, where h is the size of the mesh domain discretization. In this section, we compare the numerical solution of the Generalized Willmore graph (with $\epsilon = 0$) with a sector of the Clifford torus. Other comparisons that have been done show similar results.

In geometric topology, the Clifford torus is a torus in \mathbb{R}^4 defined by

$$\{(\cos u, \sin u, \cos v, \sin v) \in \mathbb{R}^4; 0 < u < 2\pi, 0 < v < 2\pi\}.$$

The so called Clifford torus in \mathbb{R}^3 is the stereographic projection of the actual Clifford torus in S^3 and its parametrization is given by

$$R(u, v) = ((a + \cos u) \cos v, (a + \cos u) \sin v, \sin u)$$

where $a = \sqrt{2}$. Using the coefficients of the first and second fundamental forms it can be easily shown that the profile, the mean curvature, the area element and the

weighted mean curvature of the Clifford torus in \mathbb{R}^3 are given respectively by

$$\begin{aligned}
 U &= \sin u, & H &= \frac{1}{2} + \frac{\cos u}{2(a + \cos u)} \\
 A &= \frac{1}{\sin u}, & W &= AH = \frac{1}{\sin u} \left(\frac{1}{2} + \frac{\cos u}{2(a + \cos u)} \right).
 \end{aligned}$$

For $u = 0$ and $u = \pi$ (the limits in u for the half-torus graph) the area element degenerates, $A \rightarrow \infty$, and for this reason we chose only the sector

$$\frac{\pi}{6} \leq u \leq \frac{5\pi}{6} \quad \text{and} \quad 0 \leq v \leq 2\pi.$$

The domain in the xy -plane is then given by the annulus with the following inner and outer radii

$$r_{\text{in}} = a + \cos\left(\frac{5\pi}{6}\right) = \sqrt{2} - \sqrt{3}/2, \quad r_{\text{out}} = a + \cos\left(\frac{\pi}{6}\right) = \sqrt{2} + \sqrt{3}/2.$$

The Dirichlet boundary conditions for U and W are also given by

$$\begin{aligned}
 U|_{u=\frac{\pi}{6}} &= U|_{u=\frac{5\pi}{6}} = \frac{1}{2} \\
 W|_{u=\frac{\pi}{6}} &= 2\left(\frac{\sqrt{2} + \sqrt{3}}{2\sqrt{2} + \sqrt{3}}\right) \quad \text{and} \quad W|_{u=\frac{5\pi}{6}} = 2\left(\frac{\sqrt{2} - \sqrt{3}}{2\sqrt{2} - \sqrt{3}}\right).
 \end{aligned}$$

We numerically solve (9) with the help of the FEMuS library, an open-source Finite Element Multiphysics Solver which uses automatic differentiation to evaluate the exact Jacobian in the Newton iteration scheme.

Tables 1 and 2 show the error in the L^2 norm, the error in the H^1 norm, and the corresponding convergence order, for different types of finite element families: piecewise linear, piecewise quadratic and piecewise bi-quadratic. All errors vanish as $h \rightarrow 0$. Concerning the error in the L^2 norm, the theoretical asymptotic convergence orders are recovered for each finite element family: 2 for linear, 3 for quadratic and 3 for bi-quadratic. Also for the error in the H^1 norm the theoretical asymptotic convergence orders are recovered for each finite element family: 1 for linear, 2 for quadratic and 2 for bi-quadratic.

3.3. Generalized Willmore Torus

In this section we solve the Generalized Willmore equation system (9) on the same domain and with the same boundary conditions for U and W as in the previous section, but we set the parameter $\epsilon \neq 0$. The resulting graph is not a Clifford torus anymore but a deformation of it, and an analytic solution is no longer available for comparison. From now on, we refer to each numerical solution obtained with $\epsilon \neq 0$ as *Generalized Willmore torus*.

Table 1. L^2 error and order of convergence.

	Level	Error	Order
Linear	1	0.80250526412991	0.816
	2	0.45592348448236	0.603
	3	0.30010739849527	1.055
	4	0.14447436375537	2.278
Quadratic	1	0.31005231733663	0.478
	2	0.22258445401225	1.592
	3	0.07381751192955	3.702
	4	0.00567108101373	3.694
Bi-quadratic	1	0.29624038528483	0.431
	2	0.21978351295985	1.612
	3	0.07188702858815	3.692
	4	0.00556110069160	3.687

Table 2. H^1 error and order of convergence.

	Level	Error	Order
Linear	1	1.46692032049981	0.448
	2	1.07535707689442	0.523
	3	0.74859603065803	0.717
	4	0.45556627111955	1.420
Quadratic	1	0.72593962244321	0.529
	2	0.50317937874966	1.514
	3	0.17614866253213	2.635
	4	0.02835757454658	2.023
Bi-quadratic	1	0.69164015329336	0.480
	2	0.49599585575234	1.529
	3	0.17186852938676	2.619
	4	0.02797960015931	2.016

In Fig. 1, we show the variation of the profile cross section for the Generalized Willmore torus with three different values of ϵ , namely $\epsilon = 0.001$, 0.01 and 0.03 . Note that by increasing the value of ϵ the cross section moves farther away from the one of the Clifford torus (which corresponds to $\epsilon = 0$).

Finally, in Figs. 2 and 3 we show the color maps of the profile U and the generalized curvature W for the Generalized Willmore torus with $\epsilon = 0.01$.

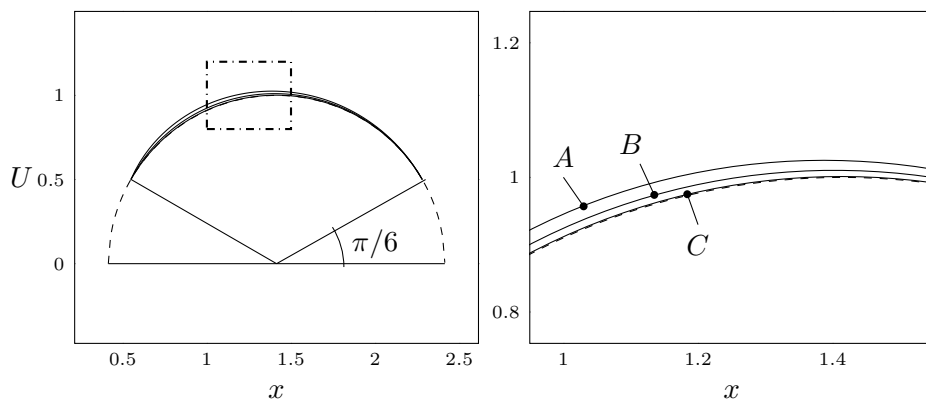


Figure 1. On the left: cross section of some computed Generalized Willmore torus surfaces for the angle range $\pi/6 \leq u \leq 5\pi/6$, for various values of ϵ . The dashed curve is the Clifford torus. The curves for $\epsilon = 0.03$ (A), $\epsilon = 0.01$ (B) and $\epsilon = 0.001$ (C) are visible on the right, in a zoom of the dash-dotted rectangle.

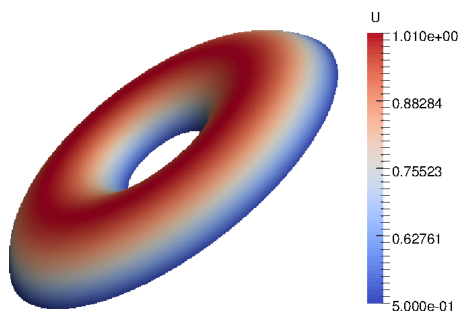


Figure 2. Generalized Willmore torus profile U with $\epsilon = 0.01$.

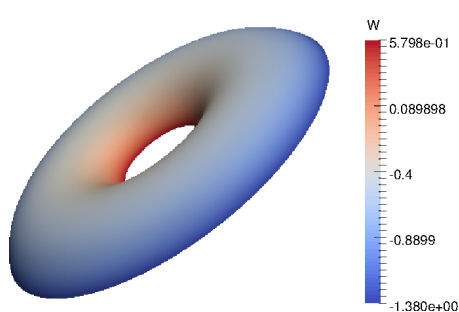


Figure 3. Generalized Willmore torus weighted curvature W with $\epsilon = 0.01$.

4. Conclusions

In this article we proposed a numerical scheme for solving a Generalized Willmore flow for graphs. We reformulated the graph evolution equation as a coupled system of nonlinear PDEs where the unknowns are the profile and the weighted mean curvature. We made use of automatic differentiation tools to compute the Jacobian in the Newton linearization of the finite element weak formulation. Finally we studied the accuracy of the algorithm by providing nontrivial steady-state numerical solutions of the Generalized Willmore flow for graphs. The present work can

be extended in several directions. The numerical scheme and the implementation presented here can be applied to time-dependent problems as well as to the case of general parametric surfaces immersed in \mathbb{R}^3 . Moreover, numerical investigations may be performed with varying values of ϵ and with different types of boundary conditions. These studies are expected to bring new interesting results which will be the subject of future works.

References

- [1] Athukorallage B., *Capillarity and Elastic Membrane Theory From an Energy Point of View*, PhD Thesis, Texas Tech University, Aug 2014.
- [2] Athukorallage B., Bornia G., Paragoda T. and Toda M., *Willmore-Type Energies and Willmore-Type Surfaces in Space Forms*, JP J. Geom. Topol. 2015, (in press).
- [3] Barrett J., Garcke H. and Nurborg R., *Parametric Approximation of Willmore Flow and Related Geometric Evolution Equations*, SIAM J. Sci. Comput. **31** (2008) 225–253.
- [4] Bobenko A. and Schröder P., *Discrete Willmore Flow*, In: Proceedings of the Third Eurographics Symposium on Geometry Processing, M. Desbrun and H. Pottmann (Eds), Eurographics Association, Aire-la-Ville 2005, pp 101–110.
- [5] Deckelnick K., Dziuk G. and Elliott C., *Computation of Geometric Partial Differential Equations and Mean Curvature Flow*, Acta Numer. **14** (2005) 139–232.
- [6] Deckelnick K., Katz J. and Schieweck F., *A C^1 -Finite Element Method for the Willmore Flow of two Dimensional Graphs*, Math. Comp. **84** (2015) 2617–2643.
- [7] Droske M. and Rumpf M., *A Level Set Formulation for Willmore Flow*, Interfaces Free Bound. **6** (2004) 361–378.
- [8] Helfrich W., *Elastic Properties of Lipid Bilayers: Theory and Possible Experiments*, Z. Naturforsch. **28** (1973) 693–703.
- [9] Hogan R., *Fast Reverse-Mode Automatic Differentiation using Expression Templates in C++*, ACM Trans. Math. Software **40** (2014) 26–41.
- [10] Ji L. and Xu Y., *Optimal Error Estimates of the Local Discontinuous Galerkin Method for Willmore Flow of Graphs on Cartesian Meshes*, Int. J. Numer. Anal. Mod. **8** (2011) 252–283.
- [11] Toda M. and Athukorallage B., *Geometric Models for Secondary Structures in Proteins*, Geom. Integrability & Quantization **16** (2015) 282–300.
- [12] Willmore T., *Riemannian Geometry*, Clarendon Press, Oxford 1996.